



Emergence of phase clusters and coexisting states reveals the structure-function relationshipDong Yu , Yong Wu, Qianming Ding, Tianyu Li, and Ya Jia ^{*}*Department of Physics and Institute of Biophysics, Central China Normal University, Wuhan 430079, China*

(Received 17 February 2024; accepted 30 April 2024; published 22 May 2024)

The Brain Connectome Project has made significant strides in uncovering the structural connections within the brain on various levels. This has led to the question of how brain structure and function are related. Our research explores this relationship in an adaptive neural network in which synaptic conductance between neurons follows spike-time synaptic plasticity rules. By adjusting the plasticity boundary, the network exhibits diverse collective behaviors, including phase synchronization, phase locking, hierarchical synchronization (phase clusters), and coexisting states. Using graph theory, we found that hierarchical synchronization is related to the community structure, while coexisting states are related to the hierarchical self-organizing and core-periphery structure. The network evolves into several tightly connected modules, with sparsely intermodule connections resulting in the formation of phase clusters. In addition, the hierarchical self-organizing structure facilitates the emergence of coexisting states. The coexistence state promotes the evolution of the core-periphery structure. Our results point towards the equivalence between function and structure, with function emerging from structure, and structure being influenced by function in a complex dynamic process.

DOI: [10.1103/PhysRevE.109.054312](https://doi.org/10.1103/PhysRevE.109.054312)**I. INTRODUCTION**

The brain neural network, consisting of numerous interconnected neurons, is one of the most complex network systems in nature [1–3]. Understanding brain function, i.e., how this intricate biological system operates, remains one of the most fundamental challenges of modern science. Network theory offers an intuitive framework to examine relationships between interconnected brain mechanisms and their bearing on behavior [4]. This provides a physical perspective to understand the complexity of the brain. By modeling the brain as a network constructed of neurons (nodes) and synapses (edges) [5], the quantitative analysis of graph theory [6] can be applied, from which the equivalence between the function and structure of neural networks can be understood. This is the general framework for the emerging field of network neuroscience [7].

The small-world phenomenon is an example of macroscopic behavior prevalent in the nervous system [8]. Small-world structure was discovered in several experimental studies of structural and functional brain networks in humans and other animals [9–12]. It reflects a balance between integrating global information and maintaining local segregation [13]. Reduction of small-worldness indicates a potential decrease in information exchange efficiency and associative memory capacity [6] and is related to neurodegenerative diseases [1]. In addition, community modularity and core-periphery structure have also been observed in the paradigm-biological rat and macaque brain connectome [14–16]. Recent work suggests that the core-periphery structure of the human brain plays a critical role in language-processing tasks [17]. As the Brain

Initiative Cell Census Network project continues to develop, brain connectomes are being uncovered from multiple temporal and spatial scales [18–23]. Therefore, it is crucial to explore the relationship between brain structure and function.

For this purpose, we constructed an adaptive neural network (ANN) that utilizes spike-time-dependent plasticity (STDP) rules to adjust the synaptic conductance between neurons. The collective dynamical behavior of the ANN is controlled by the boundaries of the plasticity rule, resulting in the phase clusters and coexisting states. The former manifests as several phase synchronization clusters in the network, while the latter is characterized by the termination of spiking activity in partially interacting neurons. Clustering of dynamics has been observed at multiple scales of brain structure and function, such as in functional magnetic resonance imaging (fMRI) data where brain networks form functional clusters [24–29]. The disruption of the clustering state may be involved in certain brain diseases [30,31]. Recent studies found stable partial synchronization patterns (phase clusters) associated with hierarchical multilayer structures in the phase oscillator model (Kuramoto model) [32–34]. We found that in ANN, the network structure spontaneously forms a community modular structure, dividing network nodes into multiple densely connected modules with sparsely intermodule connections, resulting in phase-synchronized clusters.

The coexistence of multiple brain states is another important issue in neuroscience [35]. Switching between coexisting states plays an important role in neural signaling and interactions [36–38]. Moreover, the coexistence of multiple brain states has been proposed as a fundamental mechanism for associative content-addressable memory storage and pattern recognition in neural systems [35,39–41]. We found that at higher STDP rule boundaries, the coexisting state can be promoted by phase relations and specific topologies of

^{*}Corresponding author: jiay@ccnu.edu.cn

interacting neurons. The topology is primarily determined by hierarchical self-organizing and core-periphery structure. Additionally, STDP rule boundaries can control the switching of phase-synchronization modes and coexisting states, while also influencing the network topology.

The structure of this paper is as follows: In Sec. II, we introduce an adaptive neural network composed of Hodgkin-Huxley neurons, where the plasticity of the connections between neurons is constrained by STDP rules. In addition, diagnostic tools for collective activities and network topologies are given. The main results are presented in Sec. III, while in Sec. IV, we summarize and discuss the potential implications of our findings.

II. MODEL

A. Adaptive neural network model

We consider an ANN consisting of $N = 100$ Hodgkin-Huxley (HH) neurons, where the dynamics of individual HH neural membrane potentials can be given by [42]

$$C_m \frac{dV_i}{dt} = -g_K n_i^4 (V_i - E_K) - g_{Na} m_i^3 h_i (V_i - E_{Na}) - g_L (V_i - E_L) + I_{\text{ext}} + I_i^{\text{syn}}, \quad (1)$$

where $C_m = 1 \mu\text{F}/\text{cm}^2$ is the capacity of the cell membrane, and V is the membrane potential of the neuron. $E_K = -12$ mV and $E_{Na} = 115$ mV are the Nernst potentials for the potassium and sodium ions, respectively. $E_L = 10.6$ mV is the potential at the time when the leakage current is zero. $g_K = 36$ mS/cm², $g_{Na} = 120$ mS/cm², and $g_L = 0.3$ mS/cm² denote the maximum conductance of potassium, sodium, and leakage currents, separately. The gating variables n_i , m_i , and h_i , which characterize the average proportion of working channels opening, obey the following equation [42]:

$$\frac{dy_i}{dt} = \alpha_{yi}(1 - y_i) - \beta_{yi}y_i \quad (y_i = n_i, m_i, h_i). \quad (2)$$

The α_y and β_y in Eq. (2) are the switch rates of ionic channels which depend on voltage and are described as follows:

$$\begin{aligned} \alpha_{ni} &= \frac{0.01(V_i - 10)}{1 - \exp[-(V_i - 10)/10]}, \\ \beta_{ni} &= 0.125 \exp(-V_i/80), \\ \alpha_{mi} &= \frac{0.1(V_i - 25)}{1 - \exp[-(V_i - 25)/10]}, \\ \beta_{mi} &= 4 \exp(-V_i/18), \\ \alpha_{hi} &= 0.07 \exp(-V_i/20), \\ \beta_{hi} &= \frac{1}{1 + \exp[-(V_i - 30)/10]}. \end{aligned} \quad (3)$$

The term I_{ext} is the bias current which controls the excitability level of the neuron [43]. Depending on the I_{ext} value, the HH model can exhibit silence (fixed point), bistability (coexistence of fixed point and limit cycle), and repetitive spike firing (limit cycle) [44]. Bistability in individual neuron dynamics is achieved by strategically adjusting the external input current I_{ext} , within the range that delineates the emergence of stable

and unstable limit cycles through saddle-node bifurcation (at $I_{\text{ext}} = 6.26$ $\mu\text{A}/\text{cm}^2$) and the subcritical Hopf bifurcation (at $I_{\text{ext}} = 9.78$ $\mu\text{A}/\text{cm}^2$). This range signifies the convergence of the previously mentioned unstable limit cycle with the stable fixed point equilibrium. The size of the attractor basin at the fixed point (limit ring) decreases (increases) rapidly with I_{ext} [44].

In Eq. (1), I_i^{syn} denotes the total synaptic current received by neuron i . Neurons in the network are connected by directed excitatory chemical synapses. The synaptic current takes the form

$$I_i^{\text{syn}} = \sum_{j=1(\neq i)}^N g_{ij}(t) \alpha_j [V_{\text{syn}} - V_i(t)], \quad (4)$$

$$\frac{d\alpha_j}{dt} = -\frac{\alpha_j}{\tau_{\text{syn}}} + \delta(t - t_j), \quad (5)$$

where α_j is the fraction of open receptor channels for neuron j . t_j denotes the time when the j th neuron spiking event is triggered. Then, it decays exponentially with time constant $\tau_{\text{syn}} = 3$ ms. Synapses are excitatory if V_{syn} is greater than the resting potential (around 0 mV). In this study, V_{syn} was fixed at 70 mV. Information transmission delays are inherent to the nervous system due to the limited speed at which action potentials propagate across axons [45,46]. Considering the heterogeneity of the neural network, axonal conduction delay was taken from a Gaussian distribution with a mean of 10 ms and a standard deviation of 2 ms. The set of parameters enriches the dynamics of the HH neural network [47].

B. Synaptic plasticity rules

Spike-time-dependent plasticity (STDP) is a process that produces changes in the synaptic strength. According to the STDP mechanism, the synaptic weight g_{ij} for each synapse is updated with a nearest-spike pair-based STDP rule [48]. It is calculated taking into consideration the times between the spikes of the postsynaptic neuron t_i and the presynaptic neuron t_j . The change in the excitatory synaptic weights Δg_{ij} due to the time difference $\Delta t_{ij} = (t_j - t_i)$ is given by [49,50]

$$\Delta g_{ij} = \begin{cases} P \exp(-\Delta t_{ij}/\tau_P) & \text{if } \Delta t_{ij} > 0 \\ -D \exp(\Delta t_{ij}/\tau_D) & \text{if } \Delta t_{ij} < 0 \\ 0 & \text{if } \Delta t_{ij} = 0. \end{cases} \quad (6)$$

The terms $P = 1$ and $D = 1.05$ represent potentiation and depression rate parameters, respectively, utilized to govern the extent of synaptic modification by the STDP rule. The potentiation and depression temporal windows of the synaptic modification are controlled by $\tau_P = \tau_D = 20$ ms, respectively. Each time a spike event occurs, synaptic weights are updated by Eq. (6), where $g_{ij} \rightarrow g_{ij} + r_{\text{STDP}} \Delta g_{ij}$. $r_{\text{STDP}} = 0.001$ mS/cm² is the update rate of synaptic weights. The minimal and maximal excitatory synaptic weights are considered in the interval $[g_{\text{min}}, g_{\text{max}}]$. In this study, g_{min} is set to 0, so the network structure evolves. The bounds on the STDP learning rule are determined by g_{max} , which is the parameter we focus on next.

C. Functional and structural connectivity dynamics

To investigate neuronal synchronization and symmetries, we employ the conventional Kuramoto order parameter as a diagnostic tool for the entire network, as defined by [51]

$$R_T^k(t) = \frac{1}{N} \left| \sum_{j=1}^N e^{ik\varphi_j(t)} \right|, \quad (7)$$

where “ i ” is the imaginary unit $\sqrt{-1}$ and $\varphi_j(t)$ is the neural phase associated with the spikes of each neuron j , given by

$$\varphi_j(t) = 2\pi \frac{t - t_{j,k}}{t_{j,k+1} - t_{j,k}}. \quad (8)$$

$t_{j,k}$ is the time when the k th spike happens in the j th neuron ($t_{j,k} < t < t_{j,k+1}$). After the last spike occurs of the j th neuron, $\varphi_j(t)$ is set to 0. These silent neurons are eliminated when computing $R_T^k(t)$. Briefly, we only calculate the phase synchronization and correlation between the spiking neurons. The functional connectivity (FC) between neurons is defined by phase correlations. Thus, the FC at any moment is an $N \times N$ matrix with matrix elements:

$$FC_{x,y}(t) = \frac{1}{T_0} \int_t^{t+T_0} \left| \frac{1}{2} (e^{i\varphi_x(\tau)} + e^{i\varphi_y(\tau)}) \right| d\tau. \quad (9)$$

We computed 2000 FC matrix windows in the 20 s at 10 ms intervals. Each window was calculated at a length of sliding window, $T_0 = 400$ ms, to ensure the reliability of the results. We compute the correlation of FC matrices across windows, yielding a 2000×2000 functional connectivity dynamics (FCD) matrix for each run. Correlation was measured by the Pearson correlation coefficient r_p between the matrix elements from different windows. The networks function similarly (i.e., phase locking between all neurons) when r_p is close to 1, and differently when r_p is close to 0.

Similar to the FCD method, we obtain 2000 structural connections (adjacency matrix) at 10 ms intervals and compute the Pearson correlations r_p for the different windows to obtain a 2000×2000 structural connection dynamics (SCD) matrix. The network structure is similar when the correlation is close to 1 and different at 0.

D. Network measurement

Complex networks tend to exhibit structural ordering. One such structure is known as a core-periphery structure, in which a tightly connected group of core nodes is surrounded by a sparsely connected group of peripheral nodes. Our goal is to identify this core-periphery structure by assigning nodes to either the core or peripheral group in a way that optimizes the coreness quality function [52],

$$Q_C = \frac{1}{v_C} \left[\sum_{i,j \in C_c} (g_{ij} - \gamma_C \bar{g}) - \sum_{i,j \in C_p} (g_{ij} - \gamma_C \bar{g}) \right]. \quad (10)$$

C_c is the set of all nodes in the core, while C_p is the set of all nodes in the periphery. The weight between nodes i and j is denoted as g_{ij} , and the average edge weight (averaging over all weights, including zeros) is represented by \bar{g} . γ_C is a resolution parameter controlling the size of the core; without

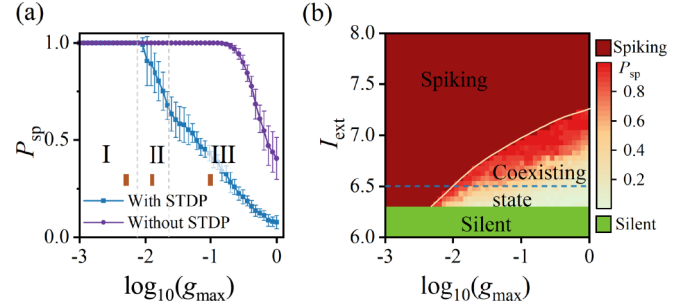


FIG. 1. Emergence of coexisting states in neuronal networks. (a) Dependence of the relative abundance of spiking neurons (P_{sp}) on STDP rule boundaries (g_{\max}). For comparison, the P_{sp} (purple line) of the static initial network is also plotted in the figure. We divide the g_{\max} parameter space into three parts based on the functional and structural properties of the system. The brown bars mark the next three cases that we focus on: $g_{\max} = 0.005, 0.012$, and 0.1 . (b) Relative abundance of spiking neurons (P_{sp}) in the two-parametric space of g_{\max} and external current I_{ext} . Solid lines indicate the boundaries between different types of collective dynamics: silent (green), spiking (red), and coexisting states.

loss of generality, we set it to 1. v_C is a normalization constant. In effect, in maximizing coreness, we seek to maximize the number and weight of intracore connections, while minimizing the number and weight of intraperiphery connections.

To evaluate the community structure in the network, we use a Leuven-like locally greedy algorithm [53] to optimize

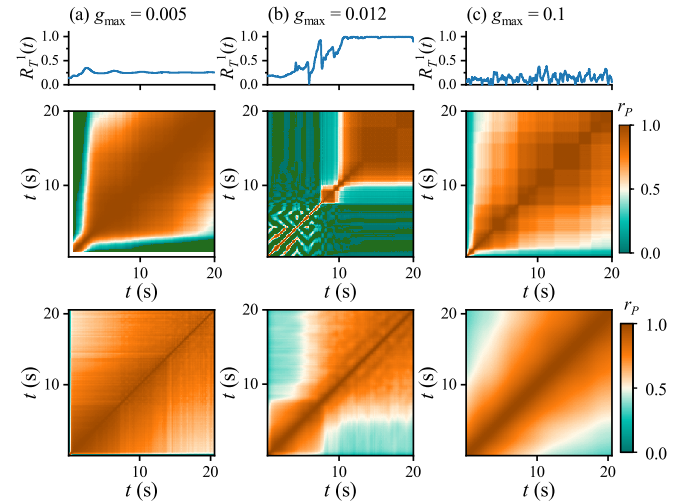


FIG. 2. STDP rule boundaries dominate the functional and structural connectivity dynamics (FCD and SCD) of the network. (a)–(c) Upper panels: Kuramoto order parameter moments for the three cases in Fig. 1 ($g_{\max} = 0.005, 0.012$, and 0.1). Middle panels: FCD matrices for the three cases in Fig. 1 ($g_{\max} = 0.005, 0.012$ and 0.1). The large brown square-shaped blocks along the diagonal indicate that the network was in phase coherence over this period. Lower panels: SCD matrices for the three cases in Fig. 1 ($g_{\max} = 0.005, 0.012$ and 0.1). r_p tends to 1 representing a constant structure. The network structure of phase clusters ($g_{\max} = 0.005$) is stable, whereas the network structure in the coexisting state ($g_{\max} = 0.012, 0.1$) is evolving.

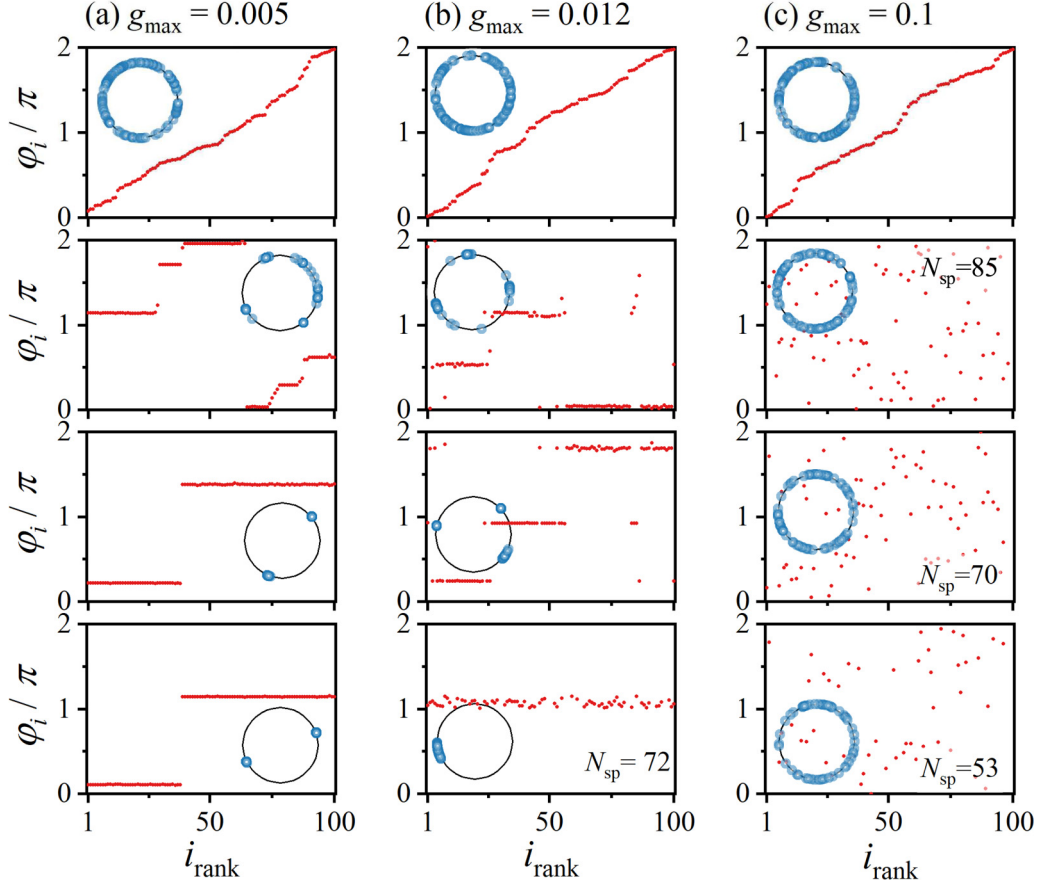


FIG. 3. Snapshots of neuronal phase distribution; from top to bottom: $t = 0.1, 1, 3,$ and 12 s. The network starts evolving with a uniformly random initial phase. For visualization, we rerank the neurons according to their phase at $t = 0.1$ s. N_{sp} is the number of spiking neurons in the network, and all neurons are spiking neurons ($N_{sp} = 100$) in the unlabeled subplot. The inset in the subplot shows the distribution of the phase in polar coordinates.

the modularity quality function,

$$Q_M = \frac{1}{v_M} \left[\sum_{i,j \in C} \left(g_{ij} - \gamma_M \frac{s_i s_j}{v_M} \right) \right] \delta_{ij}, \quad (11)$$

where C is the set of network nodes, and s_i and s_j are the summed weights of edges connected to node i and node j , respectively. γ_M is a resolution parameter controlling the size of communities which we set to 1; v_M is a normalization constant. Additionally, we employ the Kronecker delta function δ_{ij} , which equals 1 when nodes i and j belong to the same community, and 0 otherwise [52]. By maximizing the strength and number of connections within communities, modularity maximization yields a partition of the network into densely connected communities with minimal intercommunity connections.

III. RESULTS

Numerical simulations of the neuron network are carried out using the Euler method with a fixed time step of 0.01 ms. The initial state of the neuron is spiking, with a uniformly random distribution of phases between 0 and 2π . Starting from a fully connected network with randomized weights, the weights of the neural network are updated by the STDP

rule. The initial weights are distributed randomly: $\log_{10}(g_{ij}) \in [-4, g_{\max}]$. Results show that the collective dynamics in the adaptive neural network (ANN) are extremely rich: under the control of the boundaries of the STDP rule, the collective behavior emerges as phase cluster and coexisting states, which manifests as a termination of spiking activity of partially interacting neurons. First, we demonstrate the coexisting states in ANN.

A. Coexisting states in adaptive neural networks

After reaching the steady state within an evolutionary time frame of 20 s, we calculated the relative abundance of spiking neurons ($P_{sp} = N_{sp}/N$) in the network, where N_{sp} represents the number of spiking neurons and N represents the total number of neurons. In a previous study of static networks [54], coupling strength was an effective parameter for controlling coexisting states. Therefore, the STDP rule boundaries g_{\max} in ANN also significantly affect the emergence of coexisting states. Figure 1(a) demonstrates the dependence of the relative abundance of spiking neurons P_{sp} on g_{\max} . Notably, the network transitions from a spiking state to a coexisting state after g_{\max} exceeds a certain threshold ($g_{\max} \approx 0.1$), which aligns with previous results for static networks [54]. In contrast to the initial network with random weight distribution without

STDP (called initial network in the following), the STDP rule significantly reduces the silence threshold of the ANN.

Figure 1(b) shows the distribution of P_{sp} in the $(g_{\max}, I_{\text{ext}})$ parameter space. It is important to note that the collective dynamics of the network are also influenced by neuronal excitability (I_{ext}). As we mentioned in Sec. II, the limit cycle emerges after saddle-node bifurcation ($I_{\text{ext}} = 6.26 \mu\text{A}/\text{cm}^2$). Below this threshold, only a stable resting state exists in individual HH neurons, resulting in a silent network regardless of g_{\max} . However, for the parameter range of the bistable state ($I_{\text{ext}} > 6.26 \mu\text{A}/\text{cm}^2$), I_{ext} determines the relative attractor basin sizes of the fixed point and limited cycle [44]. The attractor basin size of the fixed point is negatively correlated with I_{ext} , which implies that as I_{ext} increases, neurons require larger synaptic currents to switch from the spiking to the resting state. As a result, the g_{\max} threshold (yellow solid line) is shifted towards the upper right in Fig. 1(b) as I_{ext} increases.

B. Functional and structural connectivity dynamics

The way neurons interact and the underlying network structure play a crucial role in determining the collective dynamics of the network. Previous results have shown that spike termination (neuronal electrical activity switches from spiking to resting) occurs when external stimulus and synaptic currents are in the proper phase [55]. In light of these findings, we have undertaken a deeper investigation into the relationship between the emergence of coexisting states and neuronal phases in ANN. The evolution of the Kuramoto order parameters $R_T^k(t)$ is shown in the upper panels of Fig. 2. It can be noticed that ANN undergoes a phase asynchronous \rightarrow phase synchronous \rightarrow phase asynchronous transition as g_{\max} increases.

The FCD of phase correlations between neurons is shown in the middle panels of Fig. 2. We found that there are two FCD modes. Following a brief transition stage, the network exhibits short-duration phase coherence in Fig. 2(a), and substable phase coherence in Figs. 2(b) and 2(c). In the lower panels of Fig. 2, SCD also exhibits a different pattern, which suggests that changes in function are closely related to changes in structure. These varying FCD and SCD patterns underscore the significant impact of STDP rule boundaries on network function and structure, and imply a nexus between structure and function.

After analyzing phase synchronization and correlation, we found that the ANN exhibits three distinct states: (i) asynchronous phase incoherence, (ii) synchronous phase coherent, and (iii) asynchronous phase coherent. The phase distributions for the three cases are illustrated in Fig. 3. In case (i), the neurons gradually form phase-synchronized clusters, resulting in a phase-cluster state. For case (ii), ANN initially forms phase clusters, followed by a coexisting state. The coexisting state silences part of the neurons, inducing the system to a synchronized phase-coherent state. Finally, for case (iii), the system quickly enters the coexisting state and the phase correlation is destroyed. As a result, the functional differences in ANN are dominated by the STDP rule boundaries.

To get a global view and compare the ANN with the initial network to reflect the role of STDP rules, the dependence of the Kuramoto order parameter moments on g_{\max} is plotted

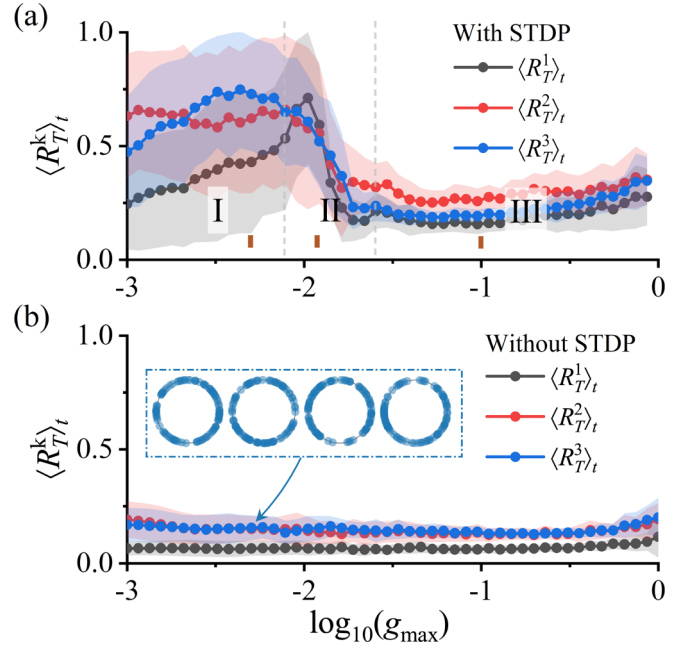


FIG. 4. Low STDP rule boundaries prompt the emergence of phase clusters. The dependence of Kuramoto order parameter moments $\langle R_T^k \rangle_t$ on g_{\max} , (a) with and (b) without STDP. The results were statistically averaged over a time period of 10–20 s. For most initial conditions, two or three phase clusters emerge spontaneously, as shown in Fig. 3(a). However, one can also observe a single phase cluster (i.e., synchronized states) for some initial conditions. Therefore, $\langle R_T^k \rangle_t$ has a large standard deviation for a small g_{\max} . The inset plots in (b) show the phase distribution for $g_{\max} = 0.005$ at the times $t = 0.1, 1, 3, 12$ s.

in Fig. 4 for the cases with and without STDP. In general, the order parameter R_T^k is sensitive to clusters with a $2\pi/k$ phase interval across the population. Therefore, high values of R_T^2 and R_T^3 and low values of R_T^1 for case (i) represent the emergence of phase-cluster states. Static networks remain in an incoherent state due to the heterogeneity introduced by randomly distributed synaptic delays and weights, regardless of g_{\max} . In contrast, STDP can facilitate the network to form phase clusters.

To further understand the underlying mechanism of phase clusters and the coexistence state, we examine the expression level of the core-periphery and the community structure of the ANN in Fig. 5. For case (i), the ANN forms a strong community structure, with several densely connected modules and sparse connections between modules in the network. This leads to the formation of several phase-synchronized clusters, as shown in Fig. 3(a). This can be further demonstrated in Fig. 6. In Fig. 6(a), after a brief transient, the neuronal phase is near stable above two phase clusters with a phase difference of π (R_T^2 approximately equal to 1). When neurons are reordered in terms of the community structure divided by Eq. (11), it is clearly observed that neurons in the same module are forming synchronized clusters. To measure the phase-clustering degree of modules in the network, we define the mean module

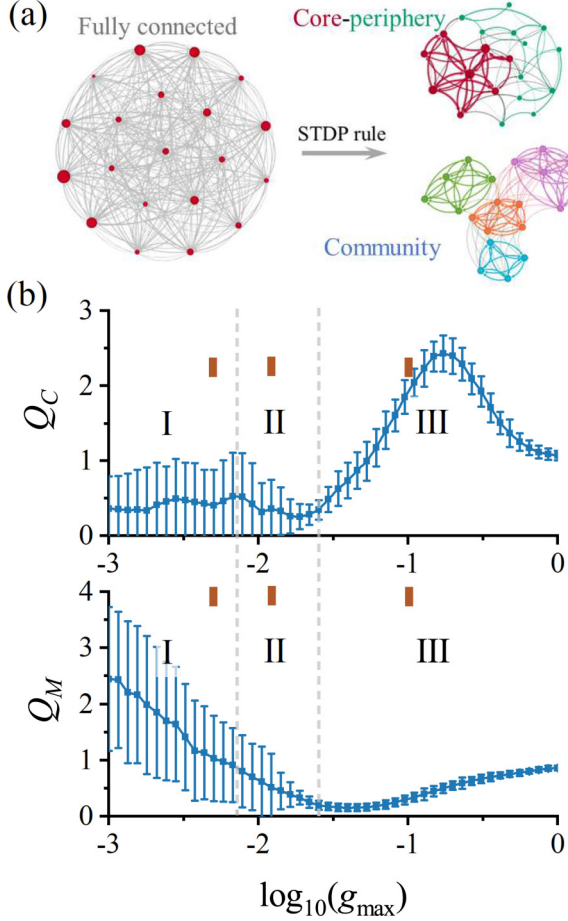


FIG. 5. STDP rules allow the network to evolve into the core-periphery and community structure. (a) Schematic of the evolution of the network structure. According to the STDP rule, fully connected networks with random edge weights evolve into sparse networks with significant core-periphery and community structures. (b) Dependence of the coreness (Q_C) and modularity (Q_M) on STDP rule boundaries (g_{\max}). Note that Q_C (Q_M) is obtained by calculating the ratio of the coreness (modularity) of the ANN to the initial network in Eqs. (10) and (11). Therefore, Q_C (Q_M) greater than 1 implies that the STDP rule makes the ANN evolve towards the core-periphery (community) structure. For case (i), the STDP rule suppresses the core-periphery structure making the community structure overexpressed. In contrast to Fig. 4, when there is only one phase cluster, the community structure is insignificant and, therefore, Q_M has a large standard deviation for small g_{\max} . For case (iii), the core-periphery structure is overexpressed.

clustering degree:

$$\sigma(t) = \frac{1}{N_M} \sum_{i=1}^{N_M} \max_{\varphi_c \in [0, 2\pi]} P_i(\varphi_c, t). \quad (12)$$

First, the network is divided into N_M subsets (modules) by Eq. (11). $P_i(\varphi_c, t)$ denotes the probability that the neuronal phase in the i th module falls between $\varphi_c - \frac{1}{2}\Delta\varphi \rightarrow \varphi_c + \frac{1}{2}\Delta\varphi$, where φ_c is the central value of the phase interval and $\Delta\varphi$ is the width. Fix $\Delta\varphi = 2\pi/180$ and find the maximum $P_i(\varphi_c, t)$ by fine-tuning φ_c . It reflects the clustering degree of the neuronal phases in the i th module. Finally, the mean

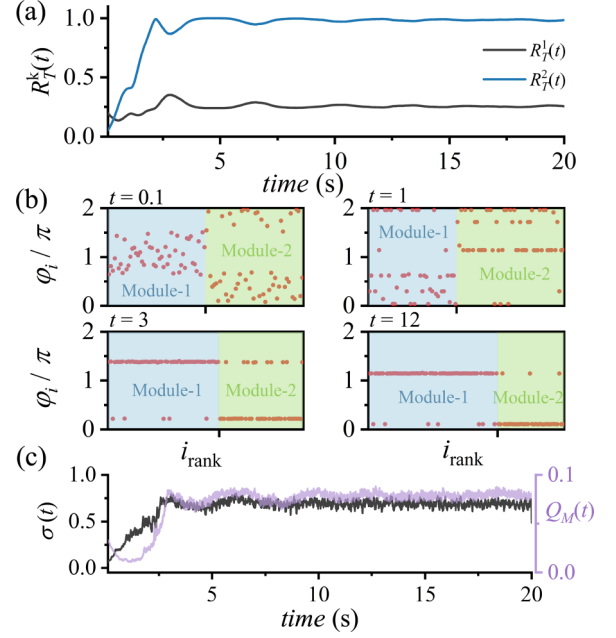


FIG. 6. ANN spontaneously forms phase clusters according to the community structure. (a) Kuramoto order parameter moments $R_T^1(t)$ and $R_T^2(t)$ for case (i) ($g_{\max} = 0.005$). (b) Snapshots of neuronal phase distribution. The data come from Fig. 3(a), but here we reorder the neuron index according to the modules divided by Eq. (11). (c) Evolution of mean module clustering degree $\sigma(t)$ and modularity $Q_M(t)$. Neuronal phases gradually evolve towards clustering, while the community structure of the network is also improved.

module clustering degree $\sigma(t)$ is obtained by averaging each module.

As shown in Fig. 6(c), $\sigma(t)$ and Q_M are maintained at a high level after undergoing a transient process. The term $\sigma(t)$ close to 1 means that neurons in the same module are synchronous, and close to 0 means that they are asynchronous. As a result, the ANN forms significant community structures and neurons of the same module are synchronized, resulting in a phase-cluster state. Interestingly, previous studies using fMRI have identified similar modular structures in brain networks [56], which may be related to brain evolution, favoring the emergence of complex dynamics and functional specialization [57].

In case (ii), the system shifts from phase clusters to a coexisting state as the community structure of the network weakens (decrease in Q_M). In case (iii), the core-periphery structure of the network is significant, with the formation of a strongly connected set of core neurons and a weakly connected set of peripheral neurons in the network. Overall, the community structure facilitates phase-synchronized cluster formation, while the core-periphery structure seems to be correlated with the emergence of coexisting states.

C. Emergence of coexisting states and core-periphery structures

In this section, we focus on how coexisting states and core-periphery structures are formed. The adjacency matrices for the three cases are given in the upper panel of Fig. 7. The

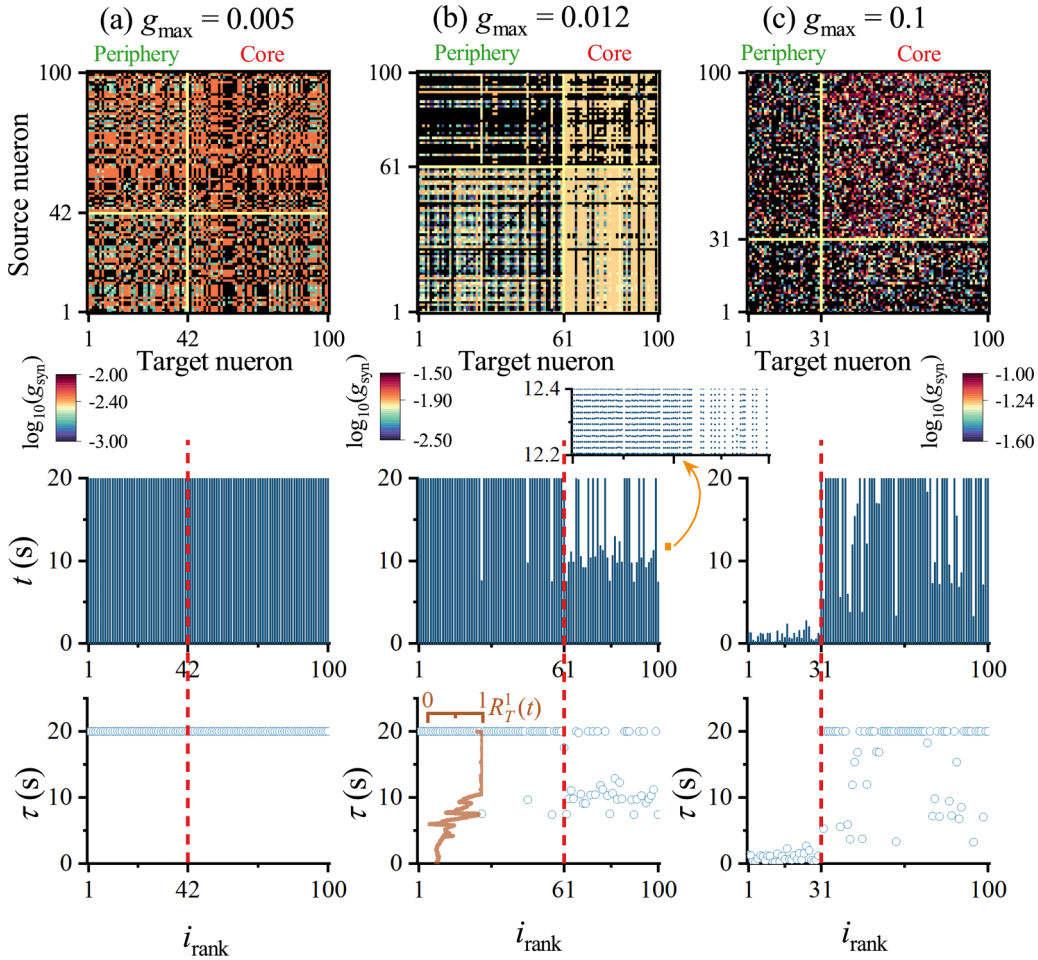


FIG. 7. Correlation of core-periphery structure with coexisting states. (a)–(c) The core-periphery structure dominates the emergence of coexisting states in the three cases ($g_{\max} = 0.005, 0.012$ and 0.1). Upper panels: adjacency matrix of the network at $t = 20$ s. Nodes are ordered according to two sets, core and periphery, respectively. Middle panels: raster plots for the three cases, with each point representing the occurrence of a spike event. Lower panels: distribution of spike termination times t in neurons. Spike termination times were defined as the time when the last spike of the neurons occurred. The inset plot in the lower panel of (b) shows the evolution of Kuramoto order parameter moments. Spike termination occurs in the phase-synchronized state.

nodes are divided according to two sets: core and periphery. For the cases $g_{\max} = 0.005$ and 0.012 , the core-periphery structure of the network is not significant ($Q_C = 0.009$ and 0.005 is small), while for the case of $g_{\max} = 0.1$, a strongly connected core set and a weakly connected periphery set are visible ($Q_C = 0.162$). The emergence of coexisting states are different mechanisms in Figs. 7(b) and 7(c). In Fig. 7(b), a clear hierarchical structure can be seen, in which the projections between the two layers (core and periphery) are directed, even though the core-periphery structure is not significant.

As in the upper panels of Fig. 7(b), the projection from the periphery to the core, i.e., the lower-right corner of the adjacency matrix, is significantly strengthened compared to the projection from the core to the periphery, i.e., the upper-left corner of the adjacency matrix. This hierarchical self-organizing structure allows core neurons to receive more excitatory presynaptic currents (EPSCs). Furthermore, in case (ii), the neurons are phase synchronized [as shown in Figs. 2(b) and 3(b)]. The phase synchronization acts like a signal rectifier amplifier that amplifies the excitatory presynaptic currents (EPSCs) of the core neuron set. Spike termination

occurs when EPSCs are in the proper phase [55]. In this intermediate state (where g_{\max} is relatively small), a few EPSCs are not enough to induce a neuron to jump from a stable limit cycle (spiking) to a fixed point (resting). Hierarchical self-organizing structures and phase-synchronous behavior amplify the EPSCs of core neurons, resulting in core neurons resting while peripheral neurons are firing.

In Fig. 7(c), the ANN is in a phase-incoherent state [as shown in Figs. 2(c) and 3(c)]. Since g_{\max} is large, when the phase relationship is appropriate, EPSCs can trigger the neuron jump from the limit cycle (spiking) attractor basin into the fixed point (resting) attractor basin, without phase-synchronized amplification. Therefore, only those sets of inappropriately phased neurons survive to form the core structure. As a result, core neurons are more spiking and peripheral neurons are more resting.

To further investigate the evolution of structure and function in ANN, we monitored the adjacency matrix every 0.1 s interval and calculated the coreness Q_C , as well as the relative abundance of spiking neurons $P_{sp,c}$ and $P_{sp,p}$ in the core and peripheral sets. The results are shown in the upper panels

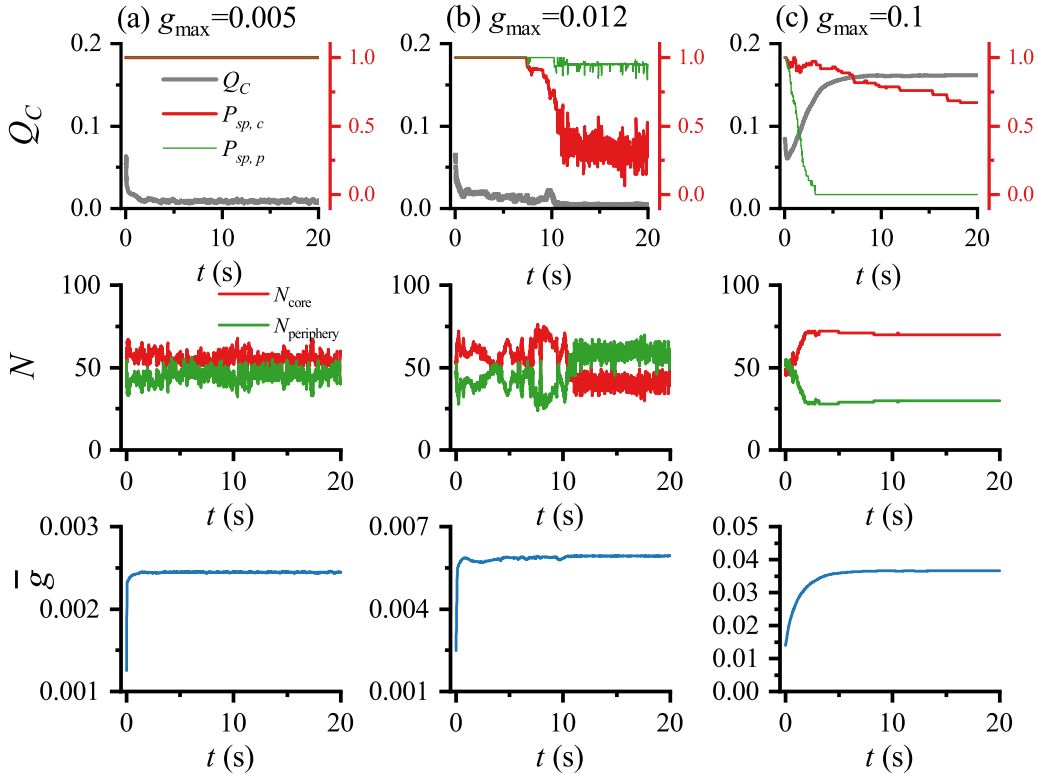


FIG. 8. Evolutionary trajectories of core-periphery structures and coexisting states. (a)–(c) Evolution of the network structure and function in the three cases of Fig. 1 ($g_{\max} = 0.005, 0.012, \text{ and } 0.1$). Upper panels: temporal trajectories of the network’s coreness Q_C and the relative abundance of spiking neurons $P_{sp,c}$ and $P_{sp,p}$ in the core and periphery. Middle panels: core and periphery subset sizes change over time in the network. Lower panels: evolution of the average coupling strength \bar{g} .

of Fig. 8. Clearly, the core-periphery structure weakens for $g_{\max} = 0.005$ and 0.012 , while it strengthens for $g_{\max} = 0.1$. Furthermore, when the STDP rule reaches equilibrium (lower panels of Fig. 8), the core-periphery structure is unstable for $g_{\max} = 0.005$ and 0.012 , but stable for $g_{\max} = 0.1$. In Fig. 8(b), the spiking neurons in the core set are constantly kicked into a resting state, while the majority of neurons in the peripheral set remain spiking. This is reversed in Fig. 8(c). These results support our analysis above.

It should be noted that in ANNs, unlike the static neural networks considered in [54,58] where the topological mechanism for realizing the coexisting state is the in-degree of nodes (i.e., the number of presynaptic neurons), the synaptic conductances are adapted by the STDP rule, which ultimately realizes a coexisting state based on the cooperation of phase relations and particular topology of the interacting neurons, where the topology primarily relies on the hierarchical self-organizing structure and the core-periphery structure. Note that we do not emphasize that topology structure is absolutely necessary for the formation of phase clusters and coexistence states. The particular structure promotes the collective dynamic behaviors of the ANN, which in turn promote the formation of the particular structure. Therefore, function emerges from structure and structure is adjusted by function.

IV. CONCLUSIONS

In this paper, we investigate the emergence of phase clusters and coexisting states in adaptive neural networks

(ANNs). Beginning with a fully connected network featuring randomized weights, the synaptic conductances of an ANN are updated via STDP rules. It is found that the network forms core-periphery and community structures. Community structure is key to forming phase clusters. The network structure spontaneously forms several tightly connected modules with sparse connections between them. As a result, phase-synchronized clusters are formed.

In addition, networks spontaneously form hierarchical self-organizing and core-periphery structures. This structure causes bistable neurons to spontaneously jump from the limit cycle (spiking) attractor basin to the fixed point (resting) attractor basin. Thus, the coexisting state is associated with the core-periphery structure. Furthermore, the STDP rules boundaries control the eventual structure of the network. Lower boundaries are more likely to result in a community structure, while higher boundaries are more likely to lead to a core-periphery structure. The STDP rules boundaries affect the network’s functionality by affecting its structure, while the network structure is adjusted by its dynamic behavior. Hence, our findings demonstrate the correlation between structure and function in ANN.

Overall, ANN can reveal equivalence between function and structure. Function emerges from structure and structure is adjusted by function, creating a complex dynamical process where structure adapts to conform with the plastic rules, and the collective behavior (function) of the network reflects the changes on the synaptic weights (structure). Beyond the scope of neuroscience, in the field of artificial intelligence, a recent

framework introduced spatially embedded recurrent neural networks, which focuses on the use of community modular and small-world networks to solve inference [59]. As the number of training epochs increases, community modular and small-world structures are significantly expressed. Therefore, understanding the relationship between structure and function in ANN is not only valuable for comprehending cognitive behavior in the human brain, but also for optimizing artificial neural networks.

ACKNOWLEDGMENTS

This work is supported by National Natural Science Foundation of China under Grant No. 12175080, self-determined research funds of CCNU from the college's basic research and operation of MOE under Grant No. CCNU22JC009, and the Central China Normal University's excellent postgraduate education innovation funding project under Grant No. 2023CXZZ129.

- [1] O. Sporns, *Dialogues Clin. Neurosci.* **15**, 247 (2013).
- [2] S. F. Muldoon, E. W. Bridgeford, and D. S. Bassett, *Rev. Sci. Rep.* **6**, 22057 (2016).
- [3] A. Zhalgalov, G. Arnulfo, L. Nobili, S. Palva, and J. M. Palva, *Netw. Neurosci.* **1**, 143 (2017).
- [4] D. S. Bassett, P. Zurn, and J. I. Gold, *Nat. Rev. Neurosci.* **19**, 566 (2018).
- [5] A. Zalesky, A. Fornito, and E. T. Bullmore, *Neuroimage* **53**, 1197 (2010).
- [6] E. Bullmore and O. Sporns, *Nat. Rev. Neurosci.* **10**, 186 (2009).
- [7] D. S. Bassett and O. Sporns, *Nat. Neurosci.* **20**, 353 (2017).
- [8] D. J. Watts and S. H. Strogatz, *Nature (London)* **393**, 440 (1998).
- [9] O. Sporns, D. Chialvo, M. Kaiser, and C. C. Hilgetag, *Trends Cogn. Sci.* **8**, 418 (2004).
- [10] D. S. Bassett and E. T. Bullmore, *Neuroscientist* **12**, 512 (2006).
- [11] J. C. Reijneveld, S. C. Ponten, H. W. Berendse, and C. J. Stam, *Clin. Neurophysiol.* **118**, 2317 (2007).
- [12] M. D. Humphries, K. Gurney, and T. J. Prescott, *Proc. Biol. Sci.* **273**, 503 (2006).
- [13] M. Rubinov and O. Sporns, *NeuroImage* **52**, 1059 (2010).
- [14] Z. Q. Liu, Y. Q. Zheng, and B. Mistic, *Netw. Neurosci.* **4**, 1181 (2020).
- [15] C. Zhou, L. Zemanová, G. Zamora, C. C. Hilgetag, and J. Kurths, *Phys. Rev. Lett.* **97**, 238103 (2006).
- [16] R. Wang, P. Lin, M. Liu, Y. Wu, T. Zhou, and C. Zhou, *Phys. Rev. Lett.* **123**, 038301 (2019).
- [17] N. H. Christianson, A. Sizemore Blevins, and D. S. Bassett, *Proc. R. Soc. A* **476**, 20190741 (2020).
- [18] E. M. Callaway *et al.* (BICCN Collaboration), *Nature (London)* **598**, 86 (2021).
- [19] K. Siletti, R. Hodge, A. M. Albiach *et al.* (Collaboration), *Science* **382**, eadd7046 (2023).
- [20] K. Whalley, *Nat. Rev. Neurosci.* **23**, 1 (2022).
- [21] Y. E. Li *et al.*, *Science* **382**, eadf7044 (2023).
- [22] D. Velmeshev *et al.*, *Science* **382**, eadf0834 (2023).
- [23] C. N. Kim, D. Shin, A. Wang, and T. J. Nowakowski, *Science* **382**, eadf9941 (2023).
- [24] M. W. Cole, D. S. Bassett, J. D. Power, T. S. Braver, and S. E. Petersen, *Neuron* **83**, 238 (2014).
- [25] G. Marrelec, A. Messe, A. Giron, and D. Rudrauf, *PLoS Comput. Biol.* **12**, e1005031 (2016).
- [26] T. Bolt, J. S. Nomi, M. Rubinov, and L. Q. Uddin, *Hum. Brain Mapp.* **38**, 1992 (2017).
- [27] Y. Zhou, K. J. Friston, P. Zeidman, J. Chen, S. Li, and A. Razi, *Cereb. Cortex.* **28**, 726 (2018).
- [28] A. Fornito, B. J. Harrison, A. Zalesky, and J. S. Simons, *Proc. Natl. Acad. Sci. USA* **109**, 12788 (2012).
- [29] N. Leonardi, J. Richiardi, M. Gschwind, S. Simioni, J. M. Annoni, M. Schlupe, P. Vuilleumier, and D. Van De Ville, *NeuroImage* **83**, 937 (2013).
- [30] E. Damaraju *et al.*, *NeuroImage: Clinical* **5**, 298 (2014).
- [31] P. J. Uhlhaas and W. Singer, *Neuron* **52**, 155 (2006).
- [32] D. V. Kasatkin, S. Yanchuk, E. Schöll, and V. I. Nekorkin, *Phys. Rev. E* **96**, 062211 (2017).
- [33] R. Berner, J. Sawicki, and E. Schöll, *Phys. Rev. Lett.* **124**, 088301 (2020).
- [34] R. Berner, J. Fialkowski, D. Kasatkin, V. Nekorkin, S. Yanchuk, and E. Schöll, *Chaos* **29**, 103134 (2019).
- [35] A. N. Pisarchik and U. Feudel, *Phys. Rep.* **540**, 167 (2014).
- [36] D. J. Angeli, E. Ferrell, Jr., and E. D. Sontag, *Proc. Natl. Acad. Sci. USA* **101**, 1822 (2004).
- [37] M. Laurent and N. Kellershohn, *Trends Biochem. Sci.* **24**, 418 (1999).
- [38] J. P. Newman and R. J. Butera, *Chaos* **20**, 023118 (2010).
- [39] C. C. Canavier, D. A. Baxter, J. W. Clark, and J. H. Byrne, *J. Neurophysiol.* **72**, 872 (1994).
- [40] A. E. Runnova, A. E. Hramov, V. V. Grubov, A. A. Koronovskii, M. K. Kurovskaya, and A. N. Pisarchik, *Chaos Solitons Fractals* **93**, 201 (2016).
- [41] J. Hertz, A. Krogh, and R. Palmer, *Introduction to the Theory of Neural Computation* (Addison-Wesley, New York, 1991).
- [42] A. L. Hodgkin and A. F. Huxley, *J. Physiol.* **116**, 497 (1952).
- [43] D. Yu, G. Wang, T. Li, Q. Ding, and Y. Jia, *Commun. Nonlinear Sci.* **117**, 106894 (2023).
- [44] D. Yu, L. J. Yang, X. Zhan, Z. Y. Fu, and Y. Jia, *Nonlinear Dyn.* **111**, 6757 (2023).
- [45] B. Sancristóbal, R. Vicente, and J. Garcia-Ojalvo, *J. Comput. Neurosci.* **37**, 193 (2014).
- [46] D. Yu, L. L. Lu, G. W. Wang, L. J. Yang, and Y. Jia, *Chaos, Solitons Fractals* **147**, 111000 (2021).
- [47] R. Vicente, L. L. Gollo, C. R. Mirasso, I. Fischer, and G. Pipa, *Proc. Natl. Acad. Sci. USA* **105**, 17157 (2008).
- [48] A. Morrison, A. Aertsen, and M. Diesmann, *Neural Comput.* **19**, 1437 (2007).
- [49] W. T. Greenough and C. H. Bailey, *Trends Neurosci.* **11**, 142 (1988).
- [50] N. Caporale and Y. Dan, *Annu. Rev. Neurosci.* **31**, 25 (2008).
- [51] Y. Kuramoto, *Chemical Oscillations, Waves, and Turbulence* (Springer-Verlag, Berlin, 1984).
- [52] M. Rubinov, R. J. F. Ypma, C. Watson, and E. T. Bullmore, *Proc. Natl. Acad. Sci. USA* **112**, 10032 (2015).

- [53] V. D. Blondel, J.-L. Guillaume, R. Lambiotte, and E. Lefebvre, *J. Stat. Mech.* (2008) P10008.
- [54] A. V. Andreev, N. S. Frolov, A. N. Pisarchik, and A. E. Hramov, *Phys. Rev. E* **100**, 022224 (2019).
- [55] M. Uzuntarla, J. Torres, A. Calim, and E. Barreto, *Neural Networks* **110**, 131 (2019)
- [56] J. D. Power *et al.*, *Neuron* **72**, 665 (2011).
- [57] O. Sporns and R. F. Betzel, *Annu. Rev. Psychol.* **67**, 613 (2016).
- [58] X. N. Li, Y. Xie, Z. Q. Ye, W. F. Huang, L. J. Yang, X. Zhan, and Y. Jia, *Chaos, Solitons Fractals* **180**, 114549 (2024).
- [59] J. Achterberg, D. Akarca, D. J. Strouse, J. Duncan, and D. E. Astle, *Nat. Mach. Intell.* **5**, 1369 (2023).